Numerical Study of the Application of a Cold Cathode Electron Gun to Materials Processing

J.I. Etcheverry *, O.E. Martínez **, N. Mingolo ***
* Departamento de Matemática, Facultad de Ciencias Exactas y Naturales
Universidad de Buenos Aires, Pabellón I, Ciudad Universitaria, 1428 Buenos Aires, Argentina
jetchev @mate.dm.uba.ar
** Departamento de Física, Facultad de Ciencias Exactas y Naturales
Universidad de Buenos Aires, Pabellón I, Ciudad Universitaria, 1428 Buenos Aires, Argentina
oem@df.uba.ar
*** Departamento de Física, Facultad de Ingeniería
Universidad de Buenos Aires, Paseo Colón 850, 1063 Buenos Aires, Argentina

A recently developed model for the application of a cold cathode electron gun to materials processing is implemented numerically to predict the expected results of irradiation of different materials in different operating conditions. This study is particularly important to establish a sound base to compare and understand the experimental results, often difficult to obtain and to interpret. In particular, maximum achieved temperatures, melted areas and depths are analyzed. It is shown that the obtained results can be essentially described by considering two dimensionless parameters: the ratio of the thermal diffusion length to the electron range, and the ratio of the incoming energy to the energy necessary to draw the material up to the melting point. In particular, changing the irradiated material at the same irradiation conditions corresponds after appropriate scaling to heat diffusion problems with source terms of the same temporal and spatial shape, but different intensities and diffusion constants. In all cases latent heats of melting and backscattering coefficients of the irradiated samples have considerable influence and must be taken into account.

Introduction

Glow discharges constitute an useful tool in many materials processing applications, because they are able to yield high energy electron beams, in relatively high pressure atmospheres, thus allowing to combine high temperature chemical reactions with electron beam irradiation. In particular, Ranea Sandoval et al. carefully characterized a pulsed cold cathode electron gun based on a high voltage glow discharge [1]. Further work demonstrated the ability of this kind of discharge to produce amorphization in $Mg_{70}Zn_{30}$ samples [2], annealing [3,4], etching of diamond films [5], etc.

Some work has been done in the mathematical modeling of this kind of discharge, and its application to materials processing [6, 7], allowing to identify new features of the produced electron beam that have been confirmed by further experimental research [8]. Among these features are the dynamic change in the discharge focusing as the discharge current and voltage change in time, the effective shortening of the electron beam energy pulse produced by the increase of the irradiated area in time, etc. A comprehensive model including these features has been developed [7], and is here implemented to analyze the temperature profiles obtained by irradiation of samples of different materials. We begin by a summary of the proposed model, and then present the numerical results and its analysis.

Basic Model

The pulsed cold cathode electron gun we consider is similar to the one developed by Ranea Sandoval et al.[1], and used by Mingolo et al.[2] to produce amorphous surfaces in $Mg_{70}Zn_{30}$ alloys. It can produce electron beam pulses of duration in the range 0.2 µs - 30 µs, with high currents up to about 900 A at accelerating voltages of about 65 kV. A schematic diagram is presented in Figure 1.

The mathematical model of the application of this pulsed cold cathode electron gun to materials processing is thoroughly described elsewhere [6, 9, 7]. We will summarize here the main features, and refer to the cited work for further details. The analysis includes a model of the electron gun discharge, in order to characterize the net energy flux impinging the sample [6], a model for the electron energy deposition inside the material [9], and the solution of the heat equation inside the irradiated material with the previously calculated energy source [7]. Assuming that the material fills the disk $-h \le z \le 0$, $r \le a$, and that the electron beam impinges normally on the face $z = 0$, the problem to solve in cylindrical coordinates is:

$$\rho c_p \frac{\partial T}{\partial t} = \frac{1}{r}\frac{\partial}{\partial r}\left(r\,\kappa(T)\frac{\partial T}{\partial r}\right) + \frac{\partial}{\partial z}\left(\kappa(T)\frac{\partial T}{\partial z}\right) + (1-\Re)\frac{i(t)\,v(t)}{S(t)}\frac{1}{R} f\left(\frac{z}{R}\right)\Theta(r(t)-r) \qquad (1)$$

where T is the temperature, and ρ, c_p, $\kappa(T)$ are the density, specific heat, and thermal conductivity of the irradiated material, respectively. The source term is given by the total energy flux incoming to the irradiated material, $(1-\Re)i(t)v(t)$, where $\Re$ is the reflectivity coefficient (fraction of backscattered energy), i(t) the discharge current, and v(t) the discharge voltage drop, multiplied by a form factor, given by the $1/R\ f(z/R)\ \Theta(r(t)-r)$, and divided by the irradiated spot area S(t). R is the electron range corresponding to the irradiated material and the actual electron energy, f is a function that describes the energy deposition profile inside the material, and Θ is the Heaviside step function. The boundary conditions to be imposed are convective and radiative loses at the surface z=0, zero flux in the line r=0 (due to the rotational symmetry around the z axis), and zero flux or room temperature at the external surface.

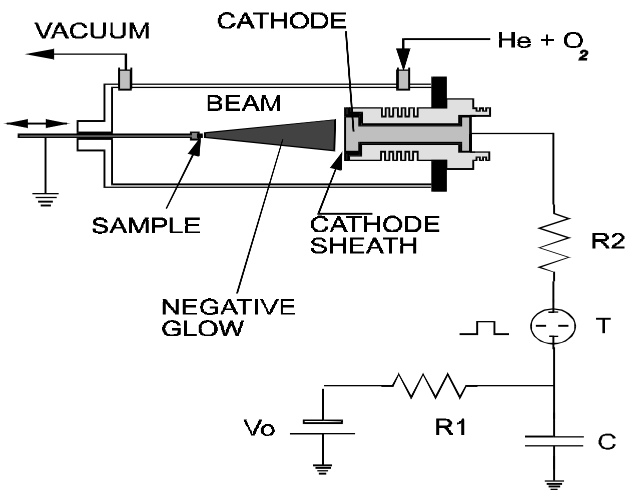

Figure 1 : Schematic diagram of the electron gun and the discharge circuit. The capacitor C is charged by the high voltage source V_0 and is discharged over the gun through the resistor R3, when the spark-gap T is triggered. The sample is held in good electrical contact with ground, and is mounted on a movable support.

The analysis of the electron beam discharge, and an simple model that predicts i(t), v(t), r(t), and S(t) in good agreement with available experimental data is given elsewhere [6]. The model is essentially based on the empirical current vs. voltage drop relation, and the fact that electrons acquire an energy equal to the voltage drop in the discharge. The electron beam self-focuses due to the strong magnetic field it generates, at a distance that depends on the voltage drop and current of the discharge. As the current and voltage drop over the gun decay in time, this focusing distance increases, and so does the irradiated area. For some processing conditions (when the electron beam is initially strongly focused), this increase in the irradiated area is the major responsible for the decrease of the incoming energy flux.

The description of the electron beam energy deposit inside the material, represented in the proposed model by the function f, the electron range R, and the reflectivity $\Re$ is obtained by means of a Monte Carlo technique [9]. It was chosen as a tool without adjustable parameters, that can produce reliable results even for complex materials, although consistent results could be obtained from standard semi-empirical formulae. The fundamental facts to bear in mind are that the shape of f is only slightly dependent on the material or the electron energy, that the electron range increases very rapidly with electron energy, at least at energies below the 100 keV range, and that at a given electron energy the reduced range (ρR) is not strongly dependent on the material.

The material is allowed to melt and vaporize, and the latent heats of melting and vaporization are implemented by means of a regularization of the enthalpy. The whole problem was solved by a semi-discretisation of the spatial variables and a numerical integration in time of the resulting ODE system [7, 10] (lines method). The integration was performed by a multistage second order adaptive Runge-Kutta method, that is specially adapted to mildly stiff problems like those that appear in the semi-discretisation of parabolic equations.

In this way the temperature profiles inside the material at different stages of the irradiation can be studied, yielding information on maximum achieved temperatures, melted pool radius and depths, vaporization thresholds, etc. as functions of the processing parameters (cathode -- sample distance, peak voltage of the discharge, gas pressure). In particular, aluminum, $Mg_{70}Zn_{30}$, stainless steel and gold samples have been studied, for electron energies in the 20 keV - 50 keV range.

Numerical Results

In order to investigate the differences between the irradiation results for different materials, we solved the model for stainless steel, $Mg_{70}Zn_{30}$, aluminum and gold, with the same discharge parameters. The assumed values of the physical constants for these materials are shown in Table 1.

Material	ρ (g/cm^3)	c_p (J/g/K)	κ (W/cm/K)	T_f (K)	T_v (K)	λ_f (J/cm^3)	λ_v (J/cm^3)
Aluminum	2.42	0.92	2.20	933	2 740	956	28 350
$Mg_{70}Zn_{30}$	2.94	0.670	1.0	613	?	666	?
Stainless steel	8.02	0.449	0.3	1 800	2 750	2 165	56 940
Gold	19.3	0.128	3.17	1 337	3 080	1 230	32 800

Table I : Physical constants of the irradiated materials [11].

Figure 2 shows the evolution in time of the discharge current, voltage drop, energy flux impinging the irradiated material surface, and irradiated spot radius. The initial voltage over the gun is 24.8 kV, the initial current about 62 A, and the cathode sample distance is assumed 29.8 cm. The strong increase of the irradiated area in time mentioned above is clearly seen, producing an energy pulse much shorter than expected from the voltage or current curves. Depending on the application this can be a desirable feature, but it is associated with a strong decrease in the melting efficiency, because most of the pulse energy is spent heating an area much wider than the actually melted area.

Figure 3 shows the temperature profiles at t = 2μs, for the four considered materials, corresponding to the discharge conditions of Figure 2. Notice that at each radial position the thermal problem is essentially one-dimensional, because the characteristic diffusion lengths are much smaller than the lateral dimensions of the irradiated spot. However, as the source term is different at each radial position, it is justified the use of a 3-D setting. Also, notice that the radius of the heated area is of the order of a couple of centimeters, while the melted spot is much smaller. As a consequence, the efficiency of the melting process is very small, because most of the energy is spent in heating an area that is not finally melt.

More detailed information is given in Figure 4, where maximum achieved temperature, melted radius and depth are plotted as a function of time for aluminum, $Mg_{70}Zn_{30}$, stainless steel and gold.

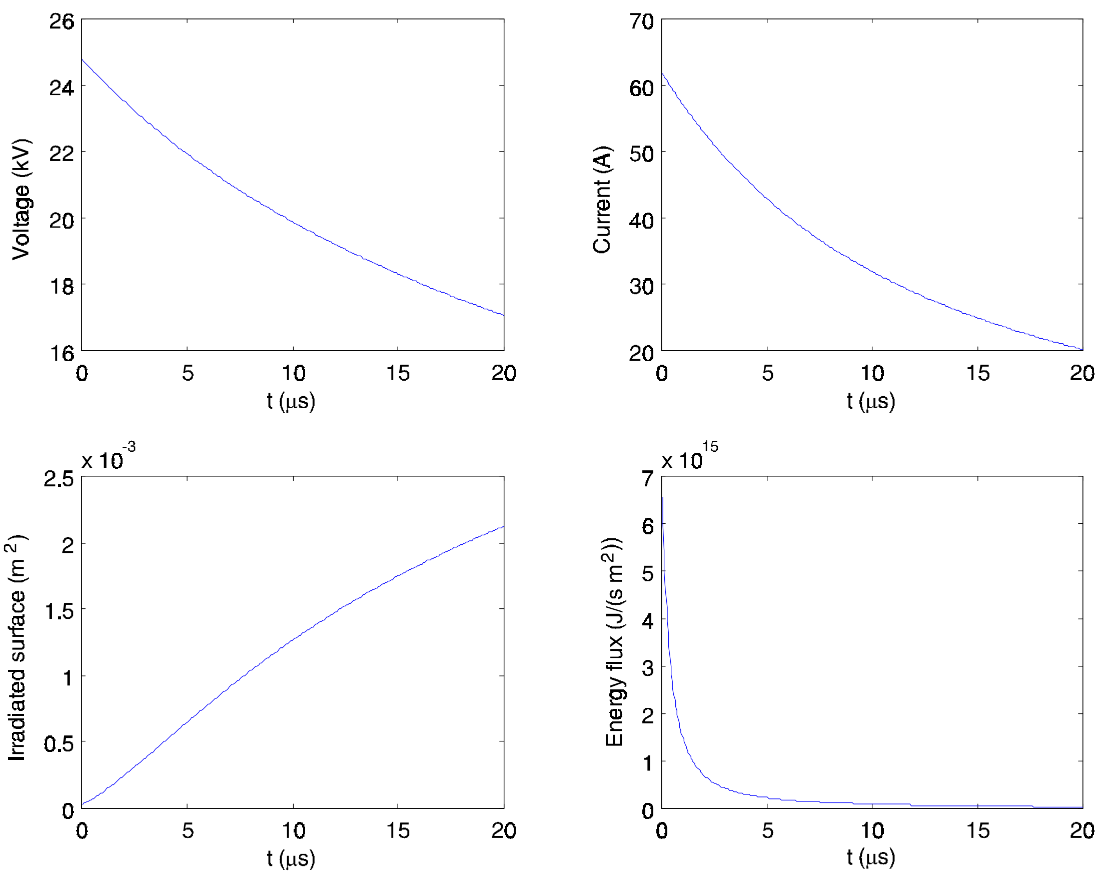

Figure 2 : Current, voltage drop, energy flux, and irradiated area as functions of time. Initial discharge voltage = 24.8 kV , cathode sample distance = 29.8 cm.

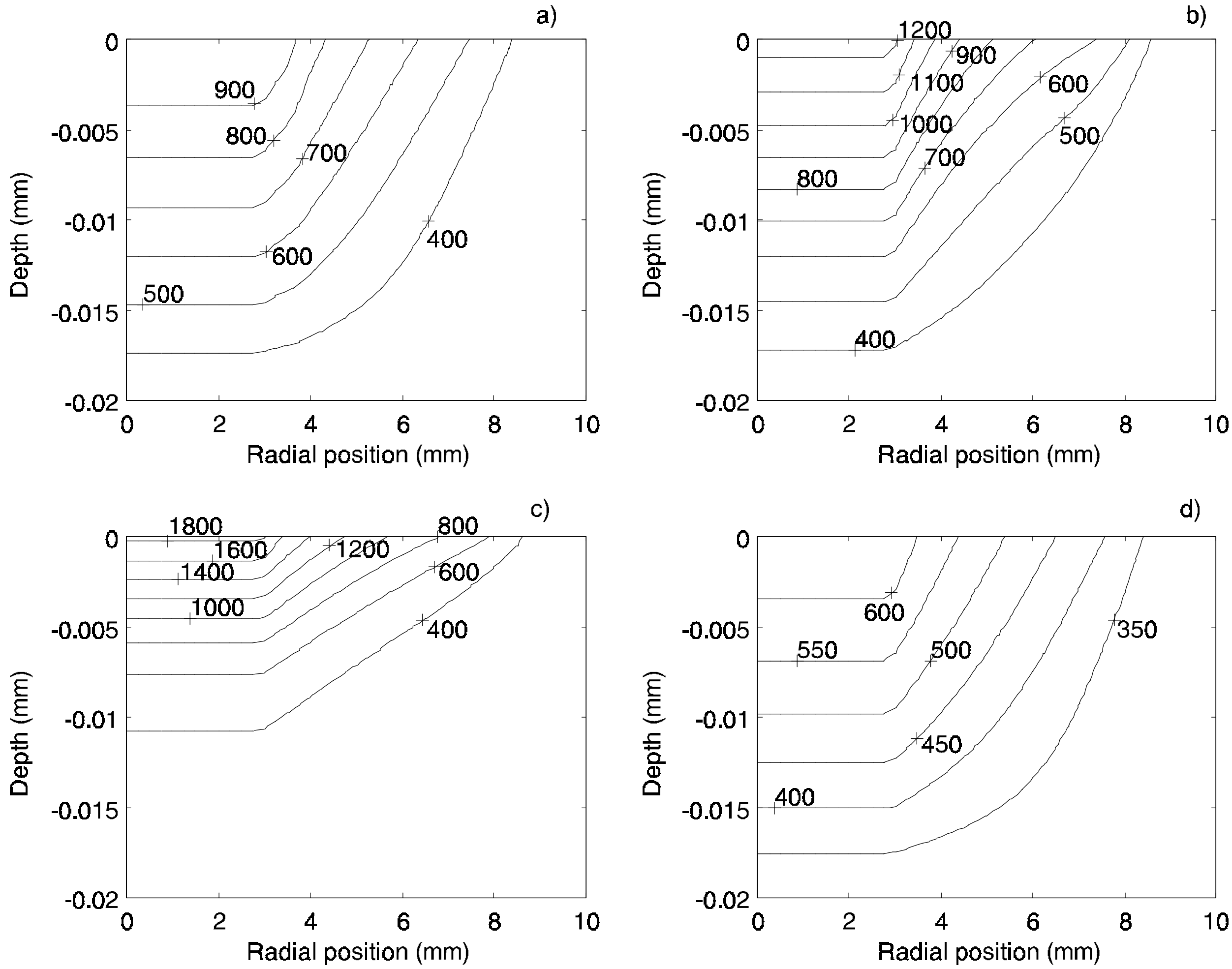

Figure 3 : Temperature level curves at t=2µs, for a) aluminum, b) $Mg_{70}Zn_{30}$, c) stainless steel, d) gold. The discharge parameters are those of Figure 2.

In order to understand the differences between the curves shown, we first observe from Figure 2 that we can assume that the electron energy is approximately constant during the energy pulse. With this assumption, the range of the beam electrons inside the irradiated material does not change significantly during the pulse, and hence the factor 1/R f(z/R) is the same for all the materials if z is normalized to R. If we further assume constant thermal conductivity, we neglect lateral diffusion, and define dimensionless variables for radial distance, time, temperature, discharge voltage and current, and irradiated area as :

$$r = r_0\, r^* \quad t = \tau\, t^* \quad T^* = (T-T_0)\,/\,T_f \quad v(t) = v_0\, v^*(t^*) \quad i(t) = i_0\, i^*(t^*) \quad S(t) = S_0\, S^*(t^*) \tag{2}$$

where r_0 is the initial spot radius, τ is a characteristic time of the energy flux, T_0 and T_f are the initial and melting temperatures respectively, v_0, i_0 are the initial values of the discharge voltage drop and current, and $S_0 = \pi\, r_0^2$ is the initial irradiated area, we can rewrite equation (1) as :

$$\frac{\partial T^*}{\partial t^*} = \frac{\kappa\,\tau}{\rho\, c_p\, R^2}\frac{\partial^2 T^*}{\partial z^{*2}} + (1-\Re)\frac{1}{R}\frac{\tau}{\rho\, c_p\, T_f}\frac{i_0 v_0}{S_0}\frac{i^*(t^*)\, v^*(t^*)}{S^*(t^*)} f\left(z^*\right)\Theta(r^*(t^*) - r^*) \tag{3}$$

Notice that the energy source term has the same spatial and temporal shape for given discharge conditions, but an intensity equal to the ratio between the energy flux incoming to the material, $(1-\Re)\, i_0\, v_0 / S_0$ and the energy flux necessary to bring a volume of depth R and unit area to fusion temperature in time τ. Taking into account the previous remark that ρR is approximately independent on the irradiated material in the range of energies of interest, and using that the factor $i^*(t^*)\, v^*(t^*)\, \tau\, f(z^*) / S^*(t^*)$ is the same for given discharge conditions, we see that the relevant factor that gives the difference between different irradiated materials is $(1-\Re) / c_p\, T_f$.

The factor multiplying the second derivative of the temperature is easily recognizable as the square of the ratio between a typical thermal diffusion length $(\kappa\ \tau\ /\rho\ c_p\ )^{1/2}$ and the electron range. The values of these dimensionless numbers corresponding to the discharge parameters of Figures 2, 3, 4, are summarized in Table II.

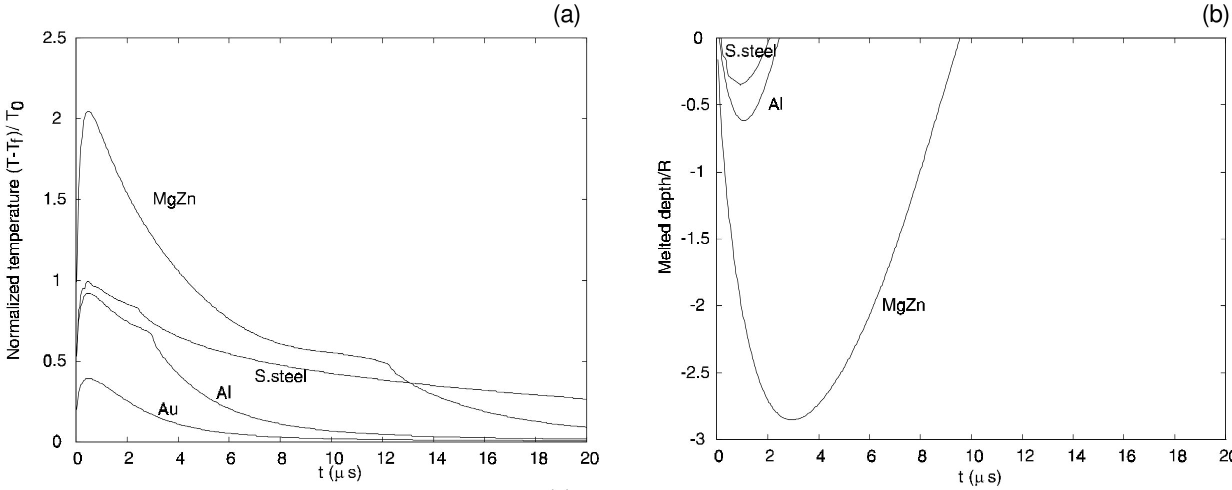

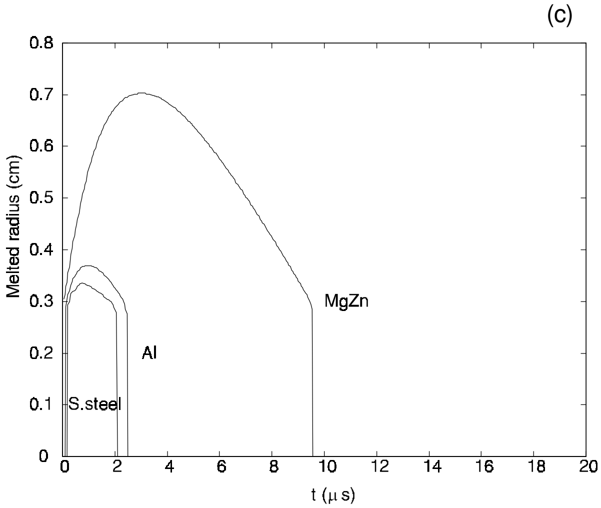

Figure 4 : (a) Normalized maximum temperature, (b) normalized melted depth, and (c) melted radius as functions of time, for the different irradiated samples. The discharge parameters are those of Figure 2.

	Aluminum	$Mg_{70}Zn_{30}$	stainless steel	gold
$\kappa\,\tau\,/(\rho\ c_p\ R^2)$	1.51	1.10	1.43	200.5
$(1-\Re)\ i_0\ v_0\ \tau/\ S_0\ R\ \rho\ c_p\ T_f$	1.74	3.35	1.68	7.45

Table II : Dimensionless parameters corresponding to the irradiation conditions of Figs. 2, 3, 4, for the considered materials.

As an example, notice that the normalized source term is approximately the same for stainless steel and aluminum, although the diffusivity coefficient is slightly greater. So, it is expected that maximum normalized temperatures are about the same, and that the corresponding melted depths are in the same proportion that the electron ranges at 24.8 keV (4.9 μm in aluminum and 1.4 μm in stainless steel). From Figure 4 a) and b) we see that this is indeed the case, although the maximum temperature is slightly smaller due to the greater thermal diffusivity, and the melted depth in aluminum is slightly larger due to the smaller latent heat of melting (see Table I).

Also, notice that in the case of $Mg_{70}Zn_{30}$ the dimensionless coefficient of the energy source term is about twice that of aluminum. Hence, it is expected that the maximum normalized temperature is a factor of 2 larger than that of aluminum. As both the latent heat of melting and the thermal diffusivity are smaller than those of aluminum, it is expected that both the normalized melted depth and radius are more than twice the corresponding of aluminum. These predictions are confirmed in Figure 4. The long lived melt can be explained from the fact that as the melting temperature is very small, the overheating of the melted region is very important, and the resolidification is not limited by the heat conduction, but by the release of latent heat. This fact, although less noticeable, is also observed in the aluminum and stainless steel cases, where a strong increase in the cooling rate is observed when the melted zone disappears (Fig. 4 (a)).

In the case of the gold sample, the dimensionless coefficient of the energy source is about four times that in aluminum, but this is compensated by the huge dimensionless diffusivity, and the gold sample does not melt at all.

Conclusions

The exposed results show that if the electron beam is strongly focused, the energy pulse duration is very short, of the order of one microsecond, and the decrease in the energy flux is mainly produced by the increase in the irradiated area, while the electron energy is practically constant [6]. In these conditions radial heat diffusion is not important, and good understanding of the heating and melting results can be obtained from the consideration of the dimensionless numbers $\kappa\,\tau/(\rho\, c_p\, R^2)$ and $(1-\Re)\dfrac{i_0\, v_0}{S_0}\dfrac{1}{R}\dfrac{\tau}{\rho\, c_p\, T_f}$. In particular, it is shown that for given irradiation conditions and different irradiated materials, the relative importance of the energy source term is essentially given by $(1-\Re) / c_p\, T_f$.

The presented examples also show the need of improving the electron gun design, in order to achieve a better melting efficiency. This conclusion explains experimental results obtained by Mingolo et al. [8], who found that irradiation of stainless steel samples with 12 J pulses produced microstructure changes in areas less than 3 mm diameter, much smaller than predicted from a simple thermal diffusion length analysis.

Finally, we stress the fact that on the basis of the described model important improvements have been made in both the design and the understanding of this kind of pulsed cold cathode electron gun.

References

1 - H.F. Ranea-Sandoval, N. Reesor, B.T. Szapiro, C. Murray, J.J. Rocca. Study of Intense electron beams produced by high-voltage pulsed glow discharges. *IEEE Transactions on Plasma Science* Vol. PS-15, No. 4, 1987.

2 - N. Mingolo, J.J. Rocca. Production of amorphous metallic surfaces by means of a pulsed glow discharge electron beam. *J. Mater. Res.* Vol. 7, No 5, 1992.

3 - C.A. Moore, J.J. Rocca, G.J. Collins, P.E. Russell, J.D. Geller. Titanium disilicate formation by wide area electron beam irradiation. *Appl. Phys. Lett.* 45, 169-171, 1984.

4 - C.A. Moore, J.J. Rocca, T. Johnson, G.J. Collins, P.E. Russell. Large area electron beam annealing. *Appl. Phys. Lett.* 43, 290-292, 1983.

5 - Koji Kobashi, Shigeaki Miyauchi, Koichi Miyata, Kozo Nishimura, J.J. Rocca. Etching of polycrystalline diamond films by electron beam assisted plasma. *J. Mater. Res.* Vol. 7, No 5, 1992.

6 - J.I. Etcheverry, N. Mingolo, J.J. Rocca, O.E. Martínez. A simple model of a glow discharge electron beam for materials processing. *IEEE Transactions on Plasma Science*, Vol. 25, N. 3, 427-432, June 1997.

7 - J.I. Etcheverry, O.E. Martínez, N. Mingolo. Numerical modeling of materials processing applications of a pulsed cold cathode electron gun. *J. Appl. Phys.* 83 (7), pp. 3856-3864, April 1998.

8 - N. Mingolo, C.R. González, J.J. Rocca, O.E. Martínez. Pulsed electron gun for surface processing of metals. *Proceedings of the First Argentina--USA Bilateral Symposium on Materials Science and Engineering, Anales de la Asociación Química Argentina,* Vol. 83 - N 5, 259-262, 1995.

9 - J.I. Etcheverry, O.E. Martínez. Monte Carlo calculation of the keV electron energy dissipation curves in compound materials. *Proceedings of the First Argentina--USA Bilateral Symposium on Materials Science and Engineering, Anales de la Asociación Química Argentina,* Vol. 84 - N 3, 221-226, 1996.

10 - C.A.J. Fletcher. Computational techniques for fluid Dynamics. Springer Verlag, Springer Series in Computational Physics, 1988.

11 - CRC Handbook of Chemistry and Physics, 73 Ed., 1992-1993, *CRC Press, Boca Raton, Ann Arbor, London, Tokyo.*